Journal of Structural Geology 31 (2009) 1458–1471

Contents lists available at ScienceDirect

Journal of Structural Geology

journal homepage: www.elsevier.com/locate/jsg

Kinematics and vorticity of flow associated with post-collisional oblique transpression in the Variscan Inner Zone of northern Sardinia (Italy)

Chiara Frassi [a,*], Rodolfo Carosi [a], Chiara Montomoli [a], Richard D. Law [b]

[a] Dipartimento di Scienze della Terra, Università di Pisa, via S. Maria 53, 56126 Pisa, Italy
[b] Department of Geosciences, Virginia Tech., Blacksburg, VA 24061, USA

ARTICLE INFO

Article history:
Received 3 April 2009
Received in revised form
24 September 2009
Accepted 5 October 2009
Available online 13 October 2009

Keywords:
Sardinia Variscan belt
Shear zones
Vorticity of flow
Petrofabrics
Oblique extrusion transpression

ABSTRACT

Quartz c-axis fabrics, vorticity of flow and deformation temperatures were analyzed in samples collected in the central sector of the Variscan inner zone in Sardinia (Italy). In order to constrain the kinematics of exhumation of medium- and high-grade metamorphic rocks during D2 post-collisional deformation, we investigated two shear belts with opposing shear senses. These shear belts are developed parallel to the trend of the inner zone which marks the boundary between two metamorphic complexes. Our data suggest that the sinistral shear belt initiated during the early stage of D2 deformation in a simple-shear-dominated regime, whereas the dextral shear belt initiated later in a pure-shear-dominated regime. We document a general non-coaxial flow regime with contemporaneous pure and simple shear components. Geometrical relationships reveal the operation of oblique extrusion during a compressive regime where the coaxial component acted sub-horizontal and orthogonal to the trend of the axial zone. Changes in the kinematics, vorticity of flow and strain geometry that occurred during D2 deformation may be related to post-collisional orogen-parallel displacement caught up in the Variscan orogeny.

1. Introduction

Crustal-scale shear zones represent the most efficient way to accommodate deformation and displacement of deep-seated crystalline rocks within collisional, transcurrent and extensional regimes. For this reason in the 1990s several numerical modelling studies (Fossen and Tikoff, 1993; Tikoff and Fossen, 1993; Robin and Cruden, 1994; Tikoff and Teyssier, 1994) investigated the relationships between finite strain, fabric evolution (foliation and lineation), and the kinematics of flow (field velocity, ISA orientation, and vorticity of flow). Most of the models assume a steady-state deformation of homogeneous materials during a general monoclinic flow, no volume loss, and parallel and undeformed boundary walls. These assumptions, however, simplified the natural constraints that generally require a more complex geometry and kinematic framework, due mainly to a partition of deformation across the shear belt and the occurrence of anisotropic starting materials (Carreras and Druguet, 1994; Druguet et al., 1997).

Following the pioneer model of Sanderson and Marchini (1984), analytical solutions predicted by numerical simulations have been introduced to explain the spatial variations in lineation, foliation and fold hinges observed in several orogens (Fossen and Tikoff, 1993, 1998; Robin and Cruden, 1994; Tikoff and Teyssier, 1994; Jones et al., 1997, 2004; Iacopini et al., 2008). However, to correlate between theoretical studies and natural examples, it is necessary to collect geometric and kinematic data from naturally occurring shear zones. For this reason, after the geometric and kinematic description of shear zones, microstructural and petrofabric analyses are necessary. In this view, vorticity analysis, deformation microstructures and quartz c-axis fabric have been frequently used to constrain deformation conditions prevailing in different tectonic settings (Law et al., 1984, 2004; Law, 1986; Wallis et al., 1993; Grujic et al., 1996; Grasemann et al., 1999; Xypolias and Koukouvelas, 2001; Sarkarinejad et al., 2008). Detecting non-coaxial components of deformation has been useful for determining the nature of first-order structures such as the South Tibetan Detachment in the Himalayan belt (Law et al., 2004), to explain the occurrence of telescoping of the metamorphic isograds (Law et al., 2008) and to compare and check theoretical models for deformation of crystallines rocks (Grujic, 2006) with natural examples in the central Himalayan belt (Carosi et al., 2007; Larson and Godin, 2009).

Our study area represents an interesting place to investigate the activity of crustal-scale shear belts during the earlier stages of post-collisional deformation of medium- and high-grade metamorphic rocks. Field observations, quartz petrofabrics analyses and vorticity

* Corresponding author. Tel.: +39 0502215809; fax: +39 0502215800.
E-mail address: frassi@dst.unipi.it (C. Frassi).

0191-8141/$ – see front matter © 2009 Elsevier Ltd. All rights reserved.
doi:10.1016/j.jsg.2009.10.001

of flow measurements allow us to identify detailed geometric and kinematics constraints on a transpression regime in which extrusion of high-grade metamorphic rocks has occurred.

2. The Sardinian Variscides

The lack of Alpine overprinting makes Sardinia island an important locality within the Southern Variscan belt for investigating deformation of Gondwana-derived terrains during and after Lower Carboniferous age continent–continent collision between Armorica and Gondwana (Carmignani et al., 1994 and references therein; Carosi et al., 2005). The sedimentary and magmatic sequences cropping out on the island were affected by folds and thrusts indicating a SW tectonic transport (Carmignani et al., 1994 and references therein; Montomoli, 2003; Carosi et al., 2005) and by a prograde Barrovian metamorphism, from anchizonal in the SW, to amphibolitic facies metamorphism in the NE (Franceschelli et al., 1982; Ricci et al., 2004) (Fig. 1).

The inner zone of the Variscan chain in Sardinia (Fig. 1) is marked by: (1) a volcanic and sedimentary sequence affected by greenschist to amphibolite facies metamorphism (the Medium Grade Metamorphic Complex: MGMC) and, (2) a Migmatitic Complex (the High-Grade Metamorphic Complex: HGMC). The latter contains Ordovician orthogneisses and mafic bodies with eclogitic (Franceschelli et al., 2007 and references therein) and granulitic (Ghezzo et al., 1979; Di Pisa et al., 1993) relicts. Deformed lenses of amphibolites with N-MORB affinity and eclogitic relicts (Cappelli et al., 1992) were also recognized in the MGMC along a km-thick mylonitic belt (Elter et al., 1990), named the Posada-Asinara Line (PAL), that divides the MGMC, to the south, from the HGMC, to the north (Fig. 1).

Structural data collected across the PAL (Fig. 1) reveal a similar structural evolution (Carosi et al., 2005 and references therein, 2009; Iacopini et al., 2008). After the D1 collisional stage (~350 Ma: Ferrara et al., 1978; 330–340 Ma: Di Vincenzo et al., 2004), the belt was affected by an orogen-parallel dextral transpressive regime (Carosi and Palmeri, 2002) developing during a D2 deformation phase (310–315 Ma: Di Vincenzo et al., 2004) responsible for most of the exhumation of high-grade metamorphic rocks (Carosi and Oggiano, 2002; Carosi et al., 2005, 2009; Iacopini et al., 2008).

The end of orogenic activity and collapse of the belt are constrained by emplacement of undeformed or weakly deformed Variscan granitoids at 280–310 Ma (Del Moro et al., 1975; Carmignani et al., 1994).

3. The SW Gallura region

In the study area the Variscan basement crops out in two different sectors, named Sector A and Sector B (Fig. 1b), divided by an early Miocene km-scale sinistral fault and by Permian volcanic sequences (Figs. 1b, 2 and 3).

The MGMC, which is only exposed in the western portion of Sector A (Fig. 2), consists of a metasedimentary sequence (micaschists, paragneisses ± quartzites) that over a horizontal distance of nearly 800 m records a strong increase in metamorphic grade moving toward the NE, from biotite up to the kyanite + biotite zone (Oggiano and Di Pisa, 1992; Ricci et al., 2004 and references therein). The HGMC is composed of migmatites, gneiss, pegmatitic veins, rare sillimanite-bearing micaschists and quartzites.

Both the MGMC and HGMC record the same polyphase deformation history with four compressive deformation phases (D1–D4,

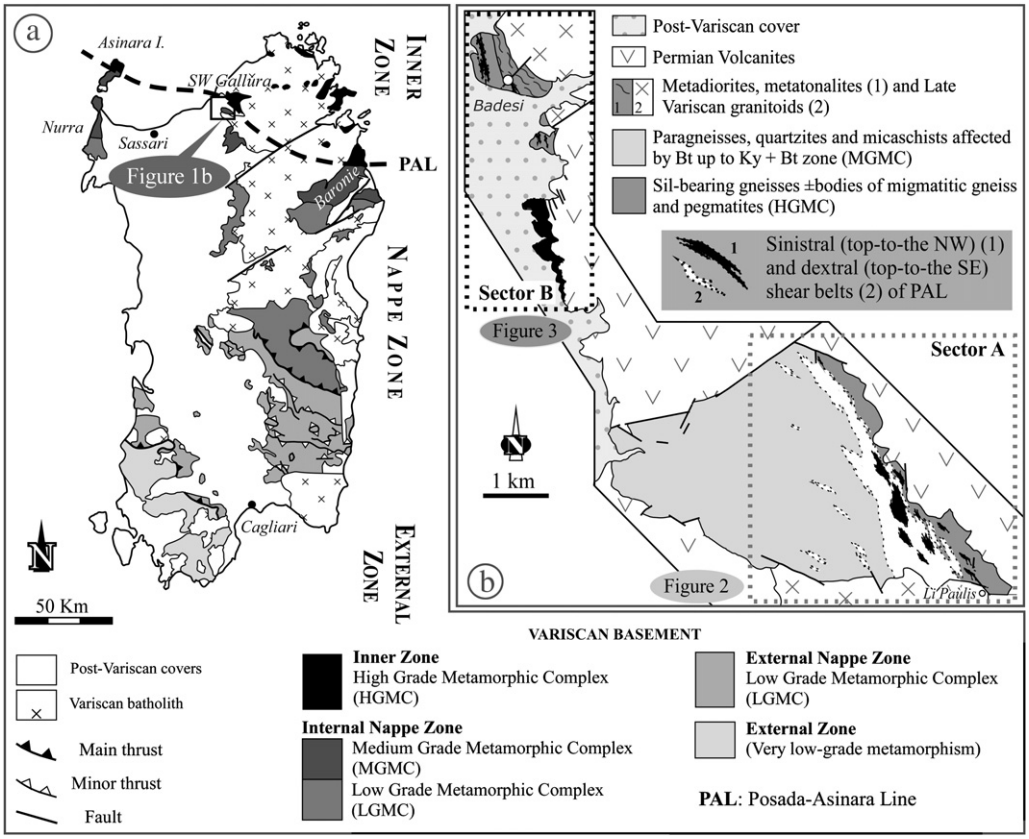

Fig. 1. (a) Geologic map of the Variscan fold-and-thrust belt in Sardinia and location of study area. (b) Geologic sketch map of study area and location of Sectors A and B discussed in text.

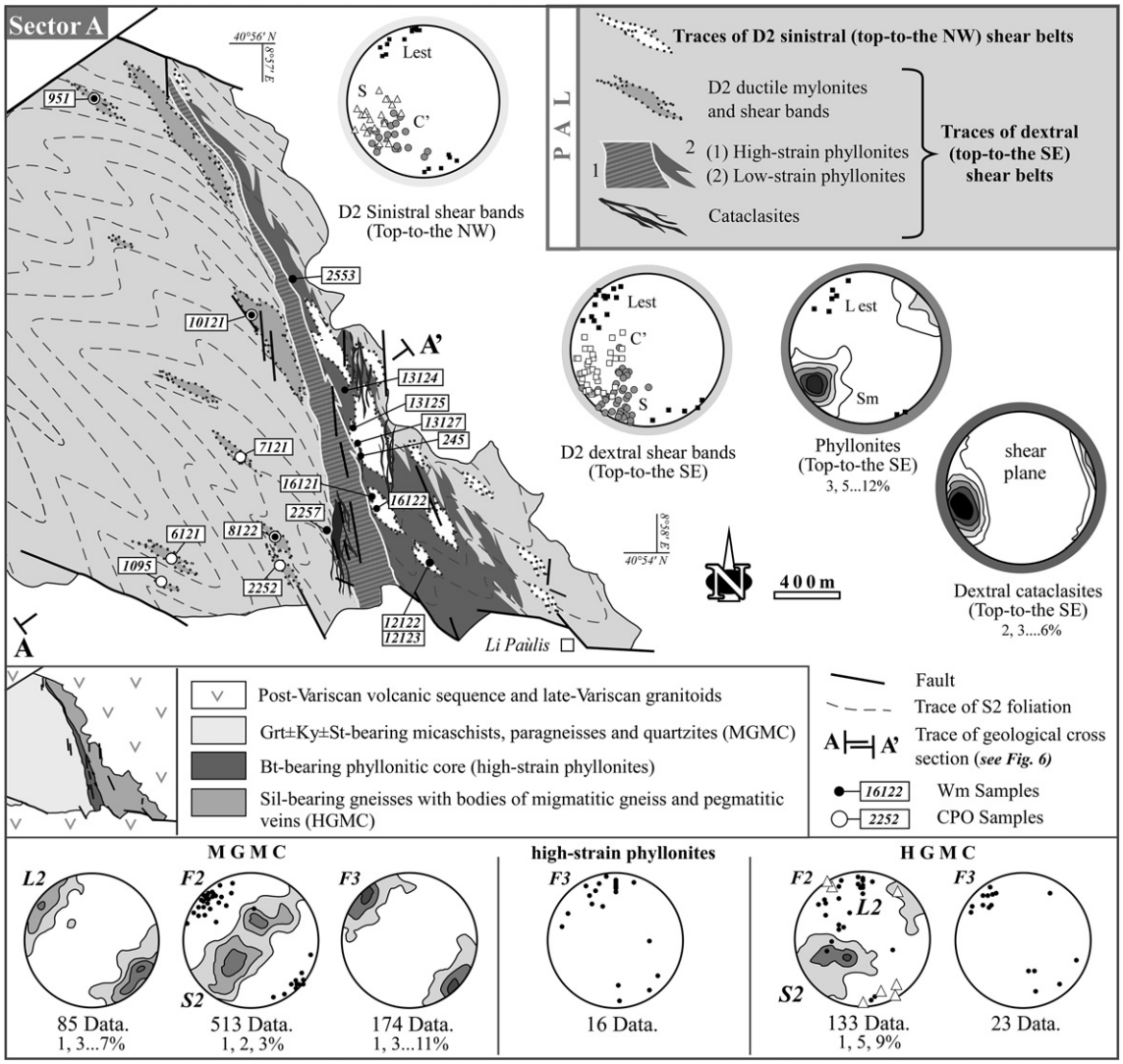

Fig. 2. Sinistral (top-to-the NW) and dextral (top-to-the SE) shear belts in Sector A and locations of samples used for CPO quartz measurements and vorticity analyses. Equal area plots of D2 and D3 structural elements are represented for the MGMC, the HGMC and the phyllonitic belt. The sinistral mylonites are preserved inside NNW–SSE trending lenses marked by irregular and gradual boundaries that coincide with a reduction of grain size and a contemporaneous increase in phyllosilicate content moving toward the phyllonites. The thickness of both the dextral mylonitic domains and the sinistral mylonitic lenses increases toward the high-strain phyllonitic belt. The dextral mylonites are distributed in thinner domains (~5 cm) in the garnet-zone, whereas close to the west margin of the phyllonites (i.e. within the kyanite + biotite zone) they reach thickness up to 100 m. The dextral high-strain phyllonitic belt that divides the MGMC and the HGMC varies in thickness from 250 m in the south to less than 50 m in the north.

Carosi et al., 2009). A later extensional brittle deformation (D5) developed during orogenic collapse. Relicts of the D1 deformation phase (mainly a penetrative S1 foliation) are recorded only in the southern portion of the MGMC because, moving toward the NE, they are progressively overprinted by the D2 deformation phase that produced a pervasive S2 foliation, tight to isoclinal F2 folds and L2 mineral lineations, all showing the same NW–SE orientation (Carosi et al., 2009). The S2 foliation has a variable dip, both toward the SW and NE, but becomes steeper near the boundary between the MGMC and HGMC, where it dips toward the NE (Fig. 6). The F2 fold axes and L2 mineral lineations usually plunge less than 25° mainly toward the NW (Fig. 2).

In Sector A, the orientation of D2 structural elements shows a sigmoidal trend in map view, varying from NW–SE to NNW–SSE to NW–SE, again moving from W to the E (Fig. 2).

The D2 deformation phase, in the study area, is characterized by the occurrence of two nearly parallel ductile and ductile–brittle shear zones showing opposite kinematics (Carosi et al., 2009): 1) a sinistral top-to-the NW shear zone, recorded exclusively in the HGMC and 2) a dextral top-to-the SE shear belt, regarded as a strand of the PAL mylonitic belt that crosscuts all of northern Sardinia (Figs. 1–3).

The two shear belts are separated by a thick sequence of dextrally sheared phyllonites that may be divided into high- and low-strain portions (Fig. 2). The high-strain phyllonites, containing less than 10% of mm-size rounded feldspar grains developed at the boundary between the HGMC and MGMC, whereas the low-strain phyllonites developed to the west of the HGMC and contain 40–45% of mm-size rounded feldspar porphyroclasts. The difference between high- and low-strain phyllonites can be mainly ascribed to an enrichment of phyllosilicate content during retrogressive mylonitization. A gradual grain-size reduction and increase in phyllosilicate content mark the transition from both the HGMC and the MGMC into the high-strain phyllonitic belt.

The belt of sinistral shear zones is preserved in sector A as metric to decametric lenses wrapped by low-strain phyllonites, composed of sheared mylonitic pegmatitic veins, mylonitic gneiss and rare mylonitic almandine + plagioclase + kyanite ± sillimanite-

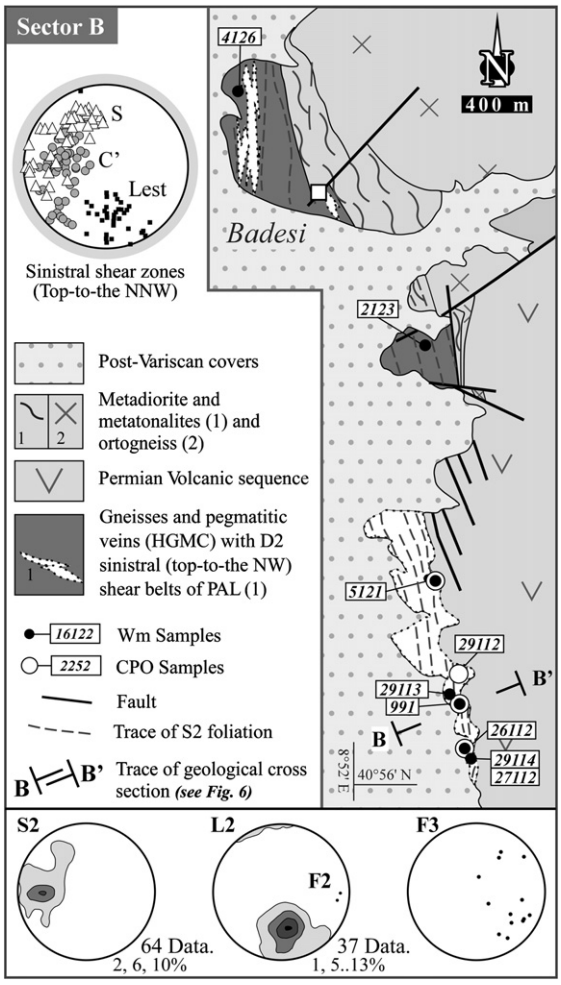

Fig. 3. Sinistral (top-to-the NW) shear belt in Sector B and locations of samples used for CPO quartz measurements and vorticity analyses. Equal area plots of D2 and D3 structural elements are shown for the HGMC.

bearing micaschists (Figs. 1b, 2). Sinistral shearing in Sector B affected fine-grained gneisses with cm-scale quartzo-feldspathic boudins, pegmatite veins and quartzites.

The presence of sinistral mylonites within the dextral shear belt, and the prolonged activity of dextral kinematics (ranging from ductile to brittle deformation conditions with the development of first phyllonites and then dextral cataclasites overprinted on both these phyllonites and the sinistral mylonites) led Carosi et al. (2009) to suggest that the sinistral shear belt started earlier.

Metric-size F3 folds with kink and/or chevron geometry affect the S2 foliation. They have steeply dipping axial planes dipping toward the E and fold axes nearly parallel to F2 structural elements. In sector A, the orientation of F3 fold axes shows in map view the same sigmoidal trend documented for the D2 structural elements. F4 folding, expressed by small-scale kink folds with N–S striking steeply dipping axial planes, marks the last compressive deformation phase. These geometric relationships constrain the activity in the dextral high-strain phyllonites to have occurred after the D3 and before the D4 deformation event.

According to Ricci et al. (2004), Frassi (2006) and Carosi et al. (2009), three distinct main metamorphic mineral assemblages can be documented. The first is related to the burial stage (D1 deformation phase) and produced in the MGMC the growth of biotite, garnet, plagioclase, kyanite and staurolite. Only biotite, garnet, plagioclase and kyanite relicts have been documented in the HGMC in Sector A. The second metamorphic mineral assemblage, recorded in the preserved mylonitic lenses of HGMC (in sector A) is characterized by prismatic sillimanite, muscovite, biotite and quartz associated with a late- to post-D2 deformation phase. Finally, replacement of chlorite + rutile on biotite and garnet crystals occurred before the D3 deformation event.

4. D2 shear belts: geometry and deformation fabric

4.1. Sinistral top-to-the NW shear belt

The sinistral shear belt crops out in the HGMC for about 8 km along a NNW–SSE trending band developed from Badesi to Li Paùlis villages (Figs. 1b, 2 and 3). The thickness of sinistral mylonites is less than 500 m in Sector A (Fig. 2), whereas in Sector B the presence of Pleistocene cover to the west, and Permian volcanic sequences to the east, leads us to assume a minimum thickness of about 200 m (Fig. 3). Mylonitic foliation is marked by S and C′ surfaces and strikes ~NW–SE with variable dips from 40 to −70° toward the NE. Lineation trends ~160–170° in Sector A, plunging less than 20° mainly toward the NW (Fig. 2), whereas in Sector B it trends ~N–S plunging generally 10–20° toward the S (Fig. 3). In the southern part of this sector the lineation plunge reaches 40–45° toward the S.

The main kinematic indicators, observed in thin sections cut perpendicular to mylonitic foliation and parallel to mineral lineation, are cm-size feldspar grains with δ- and σ-type quartz recrystallized tails (Fig. 4a), bookshelf structures in feldspar and S–C and S–C′ fabrics (Fig. 4b, c and d). In addition, at the microscopic scale, we have documented core-and-mantle structures and local grain shape preferred orientation both in quartz and feldspar, together with mica-fish and asymmetric myrmekites on feldspar. All of these microstructures indicate a sinistral sense of shear, which is confirmed by the presence of asymmetric cross-girdle quartz c-axis fabric (see Section 5).

In Sector A, the mylonitic fabric is defined mainly by S–C′ mylonites with anastomosing C′ planes which are spaced from 0.6 to 1.4 cm apart. In Sector B the mylonitic deformation is heterogeneous and strongly partitioned in cm-thick ultramylonites and bands of S–C′ mylonites of variable (2–3 to 20–30 cm) thickness. Inside these bands, the distance between individual C′ planes is generally less than 2 cm, whereas their length is about 7–10 cm. The angle between C′- and S-surfaces ranges from 20 to 30° and remains constant traced orthogonal to the shear belt boundaries.

S-surfaces are generally defined by lenticular muscovite- and biotite-fish (Ten Grotenhuis et al., 2003), sigmoidal quartz ribbons, alignment of micro-boudinaged feldspars, mosaic and domino-type fragmented feldspars (Passchier and Trouw, 2006), and fine-grained aggregates of metamorphic white mica and biotite (locally strongly replaced by chlorite). The foliation is further highlighted in sector A by relict grains of kyanite and by trails of rounded and disaggregated garnet, and in Sector B by thin layers of fine-grained dynamically recrystallized feldspar (in the thicker granoblastic quartzo-feldspathic domains) and by grain-shape alignment of quartz crystals and rare fine-aggregate of biotite, partly replaced by chlorite (in the quartzites). In Sector A, muscovite fish are locally replaced by prismatic sillimanite crystals that grew parallel and/or oblique to the S2 mylonitic foliation. C′ planes are defined by fine-grained aggregates of muscovite ± biotite and opaque minerals and, where the deformation fabric is more intense, they are further defined by planar domains of small rounded and partially recrystallized feldspar grains, and very fine-grained dynamically recrystallized quartz. Mineral lineation is highlighted by streaking of muscovite and biotite aggregates, by alignment and micro-boudinage of feldspar crystals that locally have lobate grain boundaries, and by quartz ribbons and elongate quartz–feldspar aggregates.

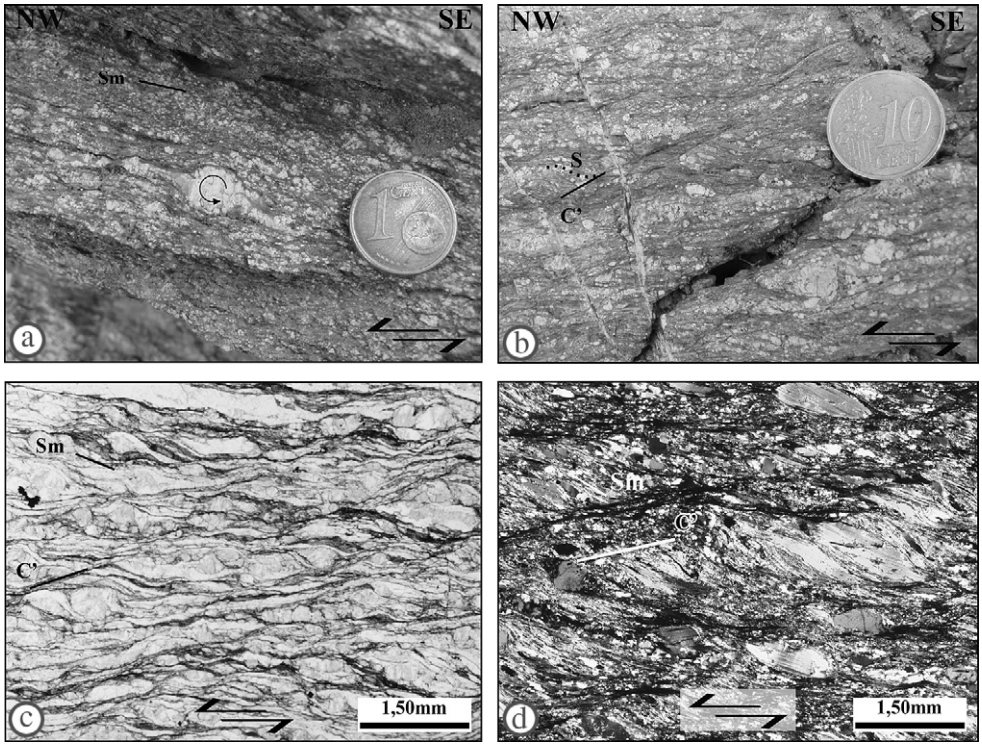

Fig. 4. Sinistral top-to-the NW shear belt. (a) Sigma plagioclase porphyroclast with ductile quartz wings from Sector B (Sm: mylonitic foliation. 2.2 cm coin for scale). (b) S–C′ fabric in Sector A. (S: mylonitic foliation; C′: shear plane; 1.8 cm coin for scale). (c) Photomicrograph of mylonitic fabric from Sector B. Sm: mylonitic foliation; C′: shear plane. (d) Photomicrograph of S–C′ fabric in micaschist lenses (S: mylonitic foliation; C′: shear plane).

4.2. Dextral top-to-the SE shear belt

The D2 dextral shear belt is strongly partitioned into conjugate S–C′/S–C mylonitic domains (less than 1 km thick) cropping out in the MGMC (Sector A) along a NW–SE trending band with a length of nearly 2 km developed parallel to the high-strain phyllonitic band (Figs. 1B and 2). In Sector A, the strike of S and C′ surfaces shows a sigmoidal trend, varying from NW–SE to NNW–SSE to NW–SE throughout the high-strain phyllonites (Fig. 2). Traced in the same direction the dip of S-surfaces changes from 30–40° to 70–80°.

The mineral lineation plunges generally less than 25°, mainly toward the N (Fig. 2). In Sector A, the strike of S and C′ surfaces shows a sigmoidal trend, varying from NW–SE to NNW–SSE to NW–SE again, throughout the high-strain phyllonites (Fig. 2). Traced in the same direction the dip of S-surfaces changes from 30–40° to 70–80°.

A dextral shear with monoclinic symmetry is indicated by feldspar and garnet grains with δ-type recrystallized tails composed of fine-grained aggregates of quartz and muscovite, foliation fish and lenticular muscovite- and biotite-fish (Fig. 5). Approaching the high-strain phyllonitic belt, the angle between C′- and S-surfaces changes from ~25–40° to ~20–25°, whereas the distance between individual shear planes decreases from 1–4 cm to less than 1.5 cm.

C′-surfaces are marked by biotite domains, local fine-grained metamorphic chlorite, recrystallized quartz and opaque minerals. Around the largest feldspar porphyroclasts extensional shear bands are developed with opposite shear senses on the opposing sides of the porphyroclasts. Mineral lineation on C′-surfaces is defined by weak streaking of biotite and muscovite domains, quartz ribbons and locally aligned kyanite crystals. The S-surfaces are defined by alignment of elongate and fragmented clasts of feldspar, staurolite and kyanite, all embedded in lepidoblastic layers of muscovite and biotite (Fig. 5c and d), and by partly recrystallized sigmoidal quartz ribbons.

The transition from the largest S–C′ mylonitic domains to the high-strain phyllonitic core is marked by: (1) an increase in phyllosilicate and opaque mineral content related to progressive disappearance of feldspars, (2) a progressive recrystallization of muscovite and biotite to a finer grain size, (3) a complete recrystallization of quartz ribbons and (4) a progressive homogenization from granoblastic to lepidoblastic layers. In the transitional zone, incipient C′-surfaces have been documented only at the microscopic scale, whereas in localities with less intense recrystallization and phyllonitization, relicts grains of feldspar have weak asymmetry and δ-type recrystallized tails of quartz.

Since the 1970s, numerous studies (Green et al., 1970; Tullis et al., 1973; Marjoribanks, 1976; Bouchez, 1977; Etchecopar, 1977; Lister and Hobbs, 1980; Schmid and Casey, 1986; Jessell and Lister, 1990; Law, 1990, and references therein; Herwegh and Handy, 1996) have suggested that quartz crystallographic fabric development is mainly controlled by the external kinematic framework and that the main girdle of quartz c-axis fabrics develops orthogonal to the flow plane. However, recent experimental work on natural quartzites (Heilbronner and Tullis, 2002, 2006) suggests that, for samples characterized by dynamic recrystallization involving grain boundary migration (Regime II of Hirth and Tullis, 1992), the main girdle rotates forward with respect to the shear plane with increasing shear strain, and is accompanied by a gradual transition from a Z-axis maximum to a Y-axis maximum density concentration in the evolving c-axis fabric.

The analysis of quartz crystal preferred orientation patterns (fabrics) in naturally deformed tectonites is a powerful tool for understanding: (1) the active slip mechanism; (2) the shape of the finite strain ellipsoid; (3) the strain magnitude and (4) the strain path (e.g. increase in simple shear). In addition, in the last ten years, quartz c-axis fabrics have been used to determine the kinematics of

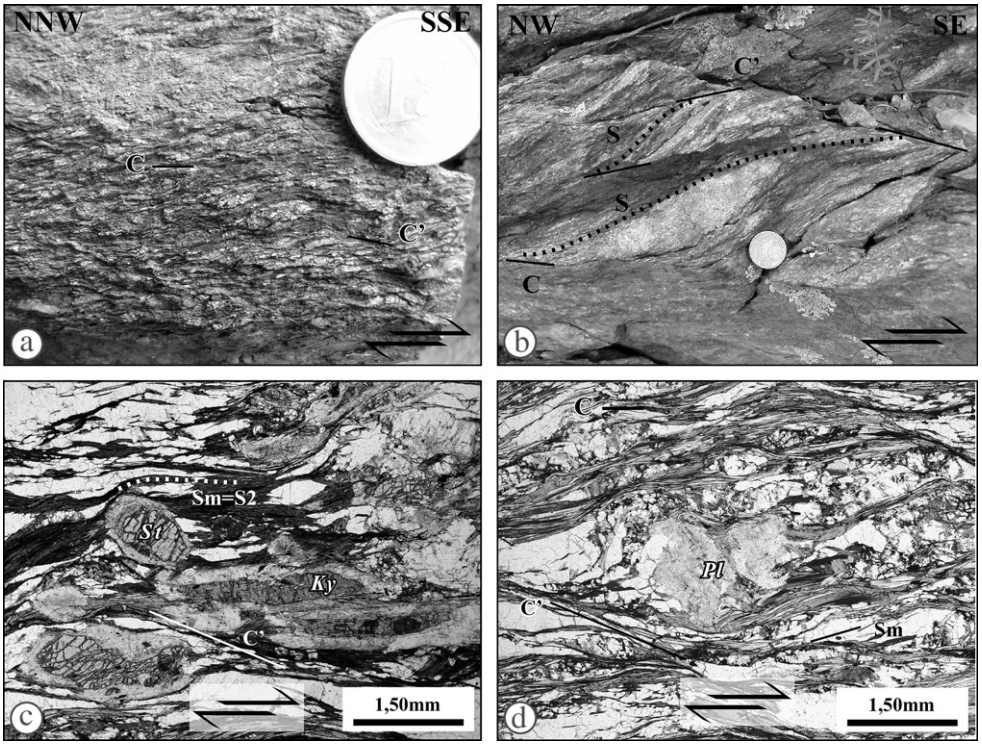

Fig. 5. Dextral (top-to-the SE) shear belt in Sector A. (a) Ky-bearing micaschists with S–C′ fabric close to high-strain phyllonitic core (C′, C: shear planes, 2.2 cm coin for scale). (b) Foliation fish in southern part of the MGMC (S: S2 foliation; C, C′: shear planes; 1.5 cm coin for scale). (c) Photomicrograph of mylonitic fabric in staurolite- (St) and kyanite- (Kt) bearing micaschists; (C, C′: shear planes). (d) Photomicrograph of mylonitic micaschist with relicts of plagioclase (Pl) and shear planes (C′) (Sm = S2: S2 mylonitic foliation).

flow (Fueten et al., 1991; Stünitz, 1991; Lana-Fùnez, 2002; Sullivan and Law, 2007; Sullivan, 2008), the vorticity number associated with flow (Wallis et al., 1993; Law et al., 2004; Xypolias, 2009) and the deformation temperature (Kruhl, 1998; Law et al., 2004; Morgan and Law, 2004). However, observed relationships between quartz crystallographic fabrics and the kinematic framework can be strongly influenced by the presence of pre-existing crystal orientations or fabrics (Vissers, 1993), the growth of phyllosilicate along preferred crystallographic orientations (Hippertt, 1994) or by dynamic recrystallization due to grain boundary migration (Heilbronner and Tullis, 2006).

In order to constrain the kinematic history of the D2 shearing event, we carried out quartz c-axis fabric measurements on 11 samples selected from different structural positions and located along a section orthogonal to the margins of the mylonitic belts (Fig. 6). All samples were cut parallel to lineation and orthogonal to mylonitic foliation. In order to obtain the most representative D2 c-axis fabrics, we choose mono-mineralic quartz ribbons not perturbed by porphyroclasts, folds or S–C′ fabrics (see Law, 1990). The measurements were collected using a universal stage mounted on an optical microscope and are presented on equal area lower hemisphere projections.

4.3. Quartz petrofabrics results

Most of the collected samples have weak asymmetric cross-girdle fabrics intermediate between Type-I and Type-II cross-girdles (Lister, 1977) indicating: 1) approximately plane strain deformation conditions (Lister and Hobbs, 1980) and, 2) the operation of non-coaxial shearing during deformation (Schmid and Casey, 1986; Law, 1990, and references therein) (Fig. 6). The asymmetric fabrics confirm the shear sense indicated by D2 micro and mesoscopic kinematic indicators, strongly suggesting that the crystal fabric was acquired during the D2 deformation phase in both shear belts. Using geometrical relationship between fabric skeletons, sample coordinates and the external kinematic framework (Tullis, 1977; Lister and Hobbs, 1980; Jessell and Lister, 1990; Takeshita et al., 1999), we argue that the measured L2 mineral lineation in both shear zone systems is true stretching lineations oriented parallel to the principal extensional direction.

Well-defined c-axis fabrics are recorded in the sinistral top-to-the NW shear belt (e.g. samples 941 and 2932, Fig. 6) where asymmetric Type-I cross-girdles qualitatively indicate accumulation of a significant component of non-coaxial shear under approximate plane strain conditions. The dominance of a pure shear component in the dextral shear belt is supported by the presence of conjugate shear bands developed at a high-angle to the central girdle of the measured c-axis fabrics (Fig. 6).

5. Deformation temperatures

To obtain complete and robust deformation temperature estimates for D2 shearing four techniques were used (Table 1): (1) the mineral assemblage on S2 mylonitic foliation, (2) the quartz and feldspar deformation microstructures (e.g. Hirth et al., 2001; Stipp et al., 2002a,b), (3) the opening angles of quartz c-axis fabric (Kruhl, 1998; Law et al., 2004) and (4) the distribution of quartz c-axis fabrics within the shear zones.

Temperatures estimated from pre-early D2 Barrovian metamorphic mineral zonation documented in the MGMC increase moving from SW toward the high-strain phyllonitic core (i.e. NE) passing from biotite up to the kyanite + biotite zone. Syn-/late-D2 metamorphic mineral assemblages in the St + Ky-bearing dextral shear zones (close to high-strain phyllonites) suggest temperatures of 450–550 °C (Carosi et al., 2009). In the western portion of the MGMC, quartz shows undulose extinction, deformation lamellae and locally straight grain boundaries, while feldspars exhibit only microfractures, indicating deformation temperatures between *c.* 350

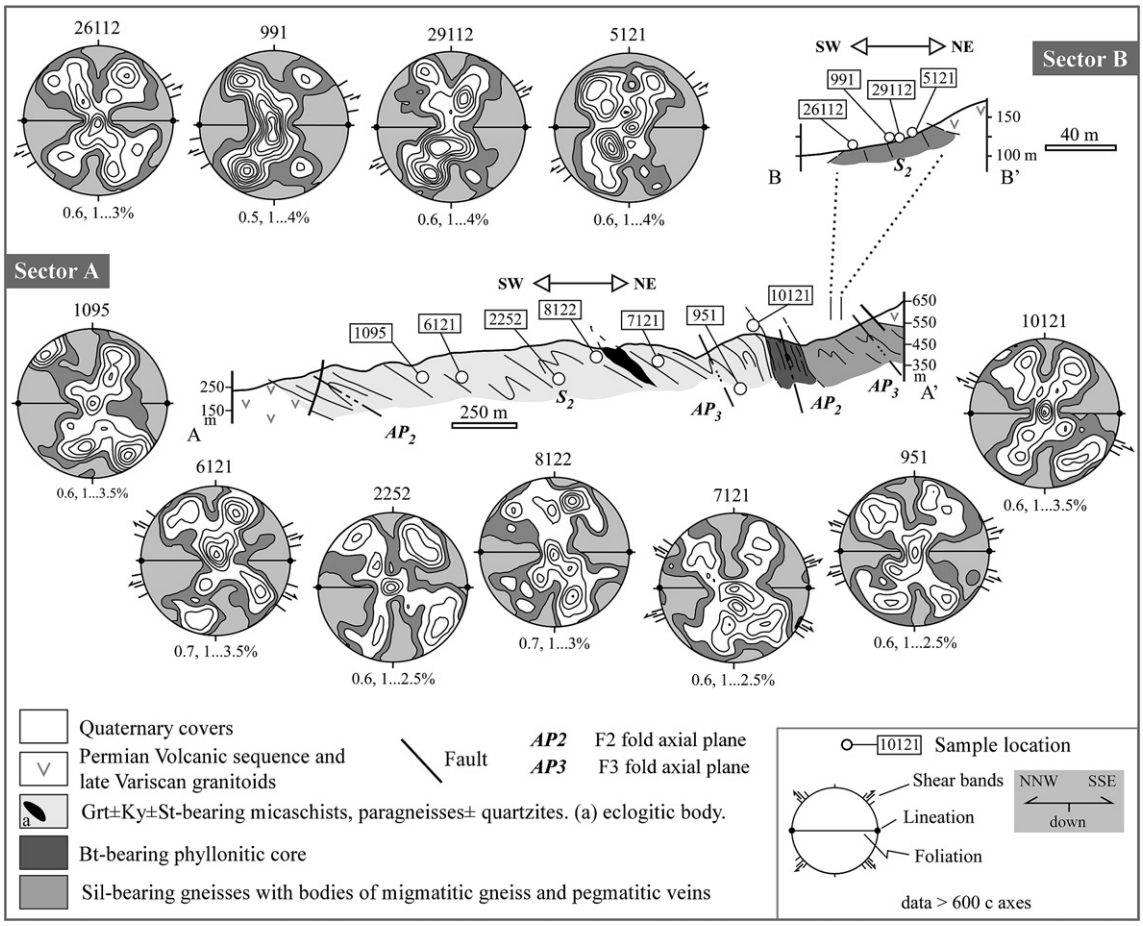

Fig. 6. Quartz c-axis fabrics from samples collected close to geological cross-section A–A′ from Sectors A and B. The fabric data are shown using lower hemisphere equal area projections.

and 400 °C. Moving toward the high-strain phyllonites, intracrystalline deformation becomes the dominant deformation mechanism. Close to the high-strain phyllonites, feldspar shows a weak grain-shape foliation, deformation twins, undulose extinction and microfracturing, suggesting temperatures higher than *c.* 450 °C. Quartz grains have lobate grain boundaries indicating intracrystalline deformation accompanied by grain boundary migration recrystallization, indicating temperatures of at least *c.* 500 °C.

Additional deformation temperature estimates can be obtained using the Kruhl's geothermometer (1998) modified by Morgan and Law (2004) and Law et al. (2004). The basic assumption made in using this thermometer is that the range in strain rates and effects of hydrolytic weakening likely to be encountered in natural deformation is encompassed in the thermometer (Law et al., 2004). In the Sardinian shear zones measured quartz c-axis fabric opening angles display a systematic variation with respect to distance from the high-strained phyllonitic core. Opening angles in the dextral top-to-the SE shear zones show a linear increase from 47° to 64° at projected distances of 360–1300 m from the phyllonitic core (Figs. 7 and 8). Plotting these data on a modified version of the Kruhl (1998) thermometer, we document a progressive rise in deformation temperature in the dextral mylonites from 370 ± 50 °C to 500 ± 50 °C traced toward the phyllonitic core (Fig. 8).

Opening angles from cross-girdle c-axis fabrics in the sinistral mylonites are generally greater than those obtained in the dextral mylonitic samples, ranging from 60° to 72° (Fig. 7). Traced toward the west, inferred deformation temperatures decrease from 550 °C to 490 °C (Fig. 8), in agreement with metamorphic temperatures obtained by the sillimanite + muscovite metamorphic mineral assemblage (T ~ 500–550 °C: Frassi, 2006; Carosi et al., 2009). These deformation temperatures are in broad agreement with temperatures estimated from quartz and feldspar deformation microstructures (Table 1).

Assuming that the high-strain phyllonitic belt may extend toward the north (i.e. in Sector B) under the Quaternary cover, we suggest a general linear relationship between opening angle/deformation temperature and structural position (Fig. 8). The deformation temperatures of 350 ± 50 °C documented in samples 10121, and the decrease in deformation temperatures traced toward the phyllonitic belt from both the dextral and sinistral shear zones (i.e. from E and W) (Figs. 7 and 8), may be related to its later activity under greenschist facies conditions.

Feldspar in the sinistral mylonite zones is deformed mainly by dislocation glide. Feldspar grains show undulatory extinction, a locally strong grain-shape foliation, bookshelf structures, rare

Table 1
Summary of deformation temperatures.

Method	Dextral shear belt		Sinistral shear belt
	W	E	
Qtz CPO opening angle	370 ± 50 °C	500 ± 50 °C	490–550 °C
Qtz c-axis distribution	≥400 °C	>400 °C	<650 °C
Mineral assemblage		450–550 °C	500–550 °C
Quartz microstructures	350–400 °C	>500 °C	450–600 °C
Feldspar microstructures	350–400 °C	>450 °C	>450 °C

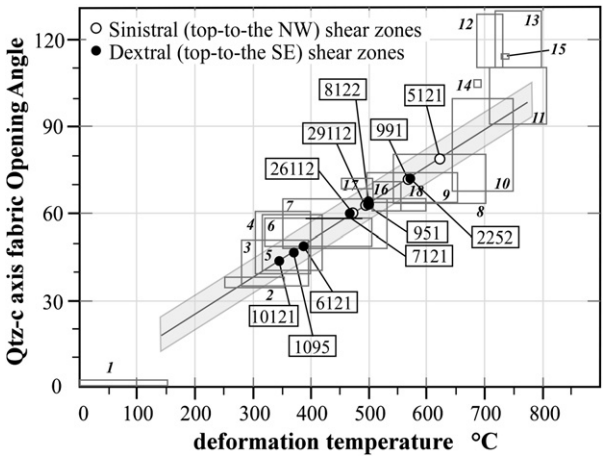

Fig. 7. Relationships between quartz c-axis fabric opening angle and deformation temperature; adapted from Kruhl (1998) and Law et al. (2004) indicate data taken from the literature for naturally deformed rocks at different metamorphic grades. 1–15: data from literature or slightly modified by Kruhl (1998); 16: Law et al. (1992); 17: Nyman et al. (1995); 18: Okudaira et al. (1995). Grey bar indicates ±50 °C geothermometer error. Data from this study are plotted and labelled.

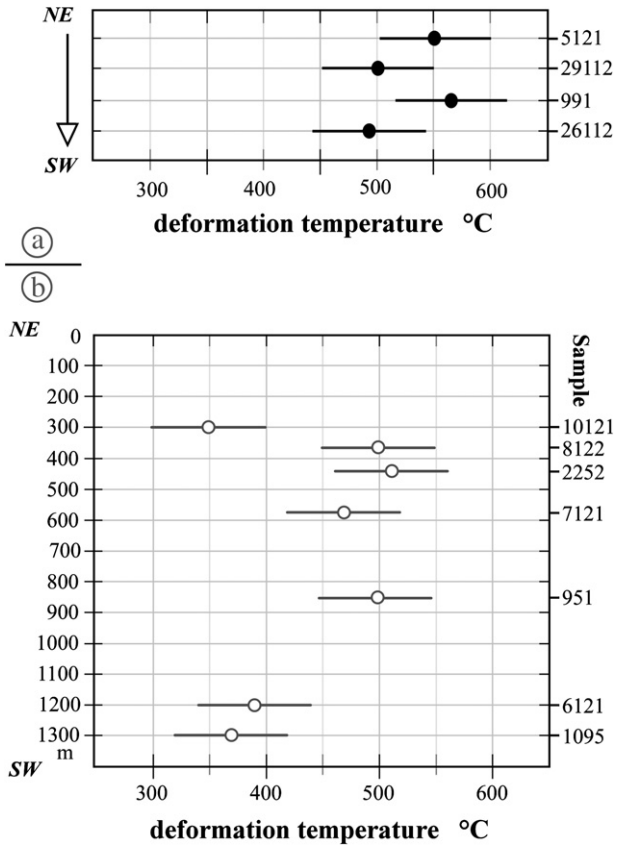

Fig. 8. Deformation temperatures obtained using the modified thermometer of Kruhl (1998) versus estimated distance from phyllonitic belts in the sinistral top-to-the NW shear belt (a) and dextral top-to-the SE shear belt (b). Samples collected along a SW–NE traverse. The exact distances for samples collected in Sector B are unknown. However we assume that they are on the east side of phyllonitic belt. Horizontal bars indicate ±50 °C error of thermometer. Non-linear relationship between deformation temperature and distance from phyllonite belts is assumed to be due to late deformation associated with motion on phyllonite belts while under greenschist facies conditions.

myrmekites (locally asymmetric), well-developed mechanical twins and, exclusively in Sector B, core-and-mantle structures. All these microstructures suggest deformation temperatures of at least *c.* 450 °C (Simpson, 1985; Pryer, 1993). Microstructures in quartz result from dislocation creep accompanied by a combination of sub-grain rotation and grain boundary migration recrystallization (Regimes 2 and 3, respectively of Hirth and Tullis, 1992). Quartz shows undulose extinction, deformation bands, weak shape preferred orientation, locally strong crystal preferred orientation, weak oblique foliation and locally developed core-and-mantle structures indicating deformation temperatures of 450–600 °C (Stipp et al., 2002a).

Density distribution variation in the c-axis fabrics suggests a dominance of prism <a> slip coupled with a combination of basal <a> and rhomb <a> slip, indicating that crystal plastic deformation occurred under moderate to high- temperature deformation conditions (T > 400 °C). However, the activity of basal <a> slip in the dextral mylonitic samples (e.g. sample 1095) indicates slightly lower deformation temperatures than in the sinistral mylonites. This trend is corroborated by deformation temperature obtained by mineral assemblages, quartz and feldspar deformation microstructures and quartz c-axis fabric opening angles.

6. Vorticity analyses

In the past two decades, a number of vorticity gauges, ranging from mesoscopic to microscopic in scale, have been proposed for quantifying the degree of non-coaxiality of flow in deformed rocks (e.g. Passchier, 1987, 1988; Wallis, 1992, 1995; Wallis et al., 1993; Simpson and De Paor, 1997; Holcombe and Little, 2001; Law et al., 2004; Jessup et al., 2007; Gomez-Rivas et al., 2007; Sullivan, 2008) using the kinematic vorticity number W_k (Truesdell, 1954; Tikoff and Fossen, 1995 and references therein). In the simple case of two-dimensional analyses W_k ranges from 0, if deformation occurs in an entirely pure shear system to 1 for a strictly simple shear regime (Means, 1994). Equal contributions of pure and simple shear occur at $W_k = 0.71$ (Law et al., 2004). However, to integrate the vorticity of the flow (W_k) over time and space it is more appropriate to consider the mean vorticity number W_m (Passchier, 1988).

To constrain the distribution of coaxial and non-coaxial shear components of deformation in the study area, and the related variation in geometry and intensity of strain, we conducted vorticity measurements on samples representative of the dextral and sinistral shear belts. Where possible, we applied two analytical methods (with different input data and starting assumptions) to the same sample in order to evaluate the reliability and consistency of results. Both methods assume a vorticity vector oriented parallel to the Y axes of finite strain (Tikoff and Fossen, 1995) and the presence of a steady-state non-coaxial flow that leads to formation of monoclinic or orthorhombic symmetry (Lin et al., 1998: Passchier, 1998). The occurrence of monoclinic symmetry has been confirmed by numerical modelling of deformation in high-strain zones by Iacopini et al. (2007).

The approximate plane strain conditions indicated by the monoclinic cross-girdle quartz c-axis fabrics in our samples and the orthogonal relationship between these cross-girdle fabrics and the sample Y-direction satisfy these assumptions, at least at the thin section scale. At the same scale, we assume homogeneous and steady-state flow.

6.1. Method I: rigid grains rotating in a viscous matrix

This method assumes that rigid porphyroclasts, without any evidence of intracrystaline deformation, rotate in a homogeneously deforming matrix reaching a stable sink orientation after some minimum finite strain accumulation. Assuming: (1) no mechanical interaction between porphyroclasts (Passchier, 1987), (2) no

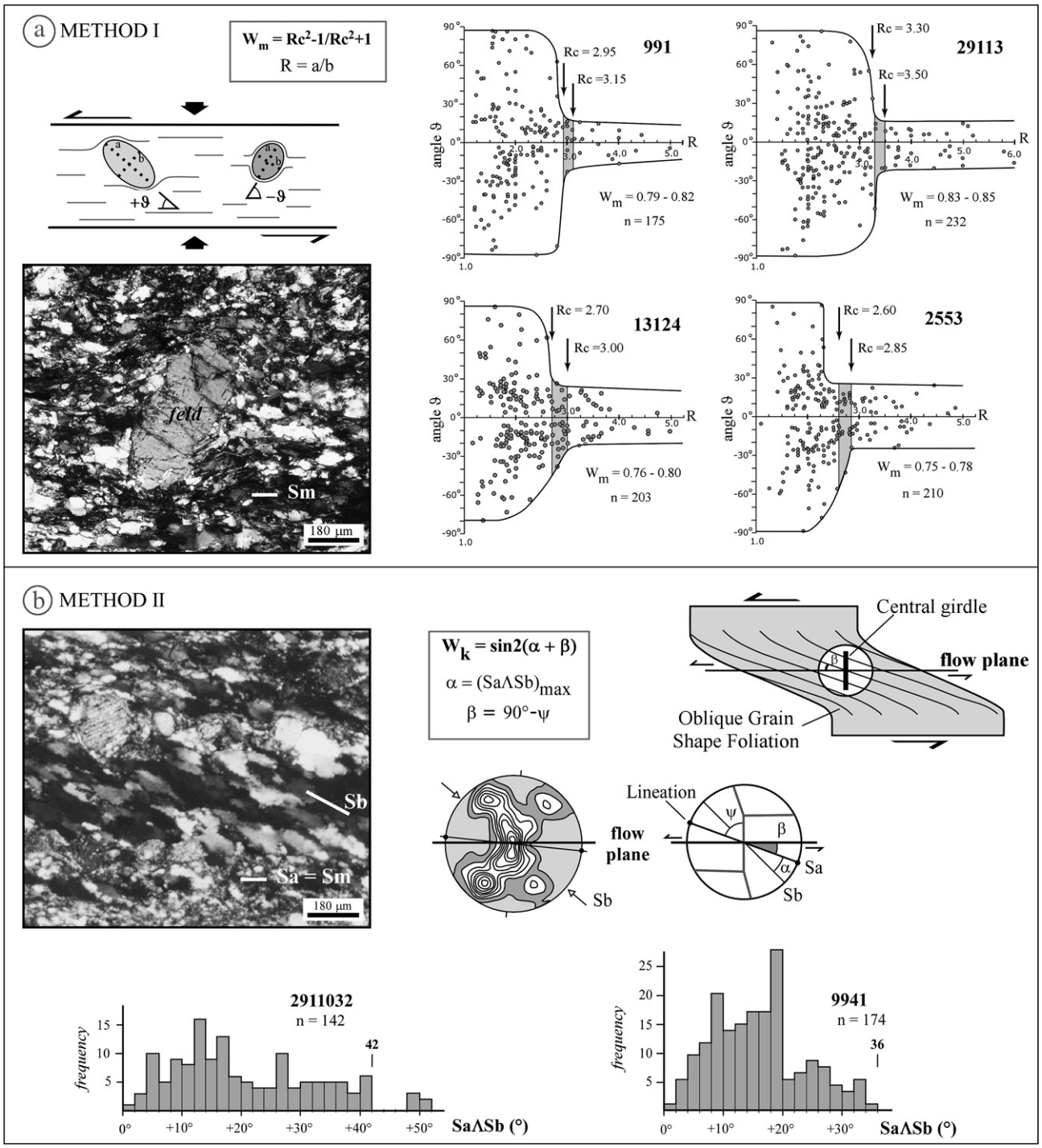

Fig. 9. Explanation of vorticity analysis techniques. (a) Geometric relationships used in Method I vorticity analyses. Illustrations include cross-polarized light photomicrograph depicting typical feldspar porphyroclast used for vorticity analyses; representative plots of porphyroclast axial ratio versus angle between foliation and long axis used to estimate R_c values (indicated by the grey field) (Law et al., 2004). ϑ is angle between long axis of porphyroclast and the main foliation, ϑ is positive if the clast long axis in inclined toward the main shear sense documented in the analyzed sample. See text for details. (b) Geometric relationships used in Method II vorticity analyses. Illustrations include angular relationship between oblique grain shape, quartz c-axis fabrics and flow plane (Wallis et al., 1993; Law et al., 2004) and shape preferred orientation histograms used to estimate W_k value, cross-light polarized photomicrograph of oblique grain shape (Sb) in sample 991. Sa: main mylonitic foliation; β: angle between the pole of central girdle of quartz c-axis fabrics and the main foliation; α: angle between the main foliation (Sa) and the oblique grain-shape foliation (Sb); ψ: angle between the central girdle of quartz c-axis fabrics and the main foliation. See text for details.

slipping interface between the matrix and porphyroclasts, (3) a sufficient strain to allow grains to reach a stable sink position and, (4) a wide initial distribution of aspect ratios among the porphyroclasts, we can estimate W_m by measuring the critical axial ratio (R_c) below which the grains continuously rotate and above which they reach a stable sink orientation (Passchier, 1987; Wallis et al., 1993) using the equation $W_m = (R_c^2 - 1)/(R_c^2 + 1)$ (Fig. 9A). According to Law et al. (2004), W_m value results are underestimated if clasts of large aspect ratio are not present. For this reason, the upper bound of the range of W_m values may in practice be closer to the

true value of vorticity. Likewise, if finite strains are low then large aspect ratio grains may not yet have reached stable sink orientations resulting in W_m being overestimated (Bailey et al., 2007, p. 100). Assuming finite strains are high enough for high aspect ratio grains to reach stable orientations, Tikoff and Fossen (1995) suggest that 2D W_m estimates of 3-dimensional monoclinic deformations overestimate the vorticity values, introducing a systematic error of at least 0.05 if sections are exactly orthogonal to the vorticity vector. Using the graphical approach suggested by Law et al. (2004), we estimated two values of W_m (W_m max and W_m min) reflecting the degree of uncertainly in determining R_c (Fig. 9a).

6.2. Method II: quartz c-axis fabrics and oblique grain shape

Based on the theoretical relationship between vorticity and the orientation of lines of zero instantaneous rotation (the flow aphophyses) and instantaneous stretching axes (ISA) (Passchier, 1988), Wallis (1995) has argued that the orientation of elongate dynamically recrystallized quartz grains, relative to the central girdle of the associated quartz c-axes fabric in a given sample, can be used to estimate the kinematic vorticity number W_k (Fig. 9b). According to Wallis (1995), the oblique grain shape in quartz aggregates is produced by a progressive rotation and stretching of recrystallized grains that nucleate with their long axes parallel to the instantaneous stretching axes (ISA). As a consequence, the maximum angle (α) recorded between the long axis of dynamically recrystallized grains and foliation identifies the approximate ISA orientation (Fig. 9b). In general shear flow, it is assumed that the flow plane is oriented perpendicular to the central segment of the associated single or cross-girdle quartz c-axis fabric. Foliation is oriented at an angle β to the pole to the central segment of the quartz c-axis fabric; i.e. β is the angle between foliation and the inferred shear plane. Measuring the angles α and β, we can estimate W_k using the equation $W_k = \sin 2(\beta + \alpha)$ (Wallis, 1995) (Fig. 9b). However, it should be noted that if the central part of the quartz c-axis fabric girdle rotates in the shear direction with progressive shearing, as produced in recent general shear experiments by Heilbronner and Tullis (2006), then Method II vorticity results will overestimate W_k. Potential supporting evidence for this phenomenon and its influence on vorticity calculations has recently been described from the Moine thrust of NW Scotland by Law et al. (2007) and Law (in press).

6.3. Results of vorticity measurements

Vorticity estimates from the dextral and sinistral shear belts of the study area obtained using the two analytical methods are shown in Fig. 10 (see Data Repository for additional Rigid Grain plots). W_m estimates for the sinistral shear belt range between 0.68 and 0.88 using Method I, and from 0.62 to 0.98 using Method II. The different – but overlapping – range of W_m values obtained using the two methods may be a reflection of a number of factors including: a) different assumptions built into the two methods, b) different analytical problems associated with obtaining basic input data for the two methods, c) different methods recording different spatial and/or temporal parts of the total strain history. Keeping in mind these uncertainties, both methods indicate a major component of simple shear relative to pure shear deformation. In detail, Method I W_m estimates from the northern outcrops of sinistral mylonites (Sector B, Figs. 1b and 3) indicate a simple shear component representing 59–69% of the total deformation ($W_m = 0.79$–0.88 with average value of 0.83). In contrast, Method II W_k values from the same samples indicate a simple shear component of 43–88% (average W_k value of 0.80) (Fig. 10). In the southern sinistral mylonitic outcrops (Sector A, Figs. 1a and 2), Method I analyses

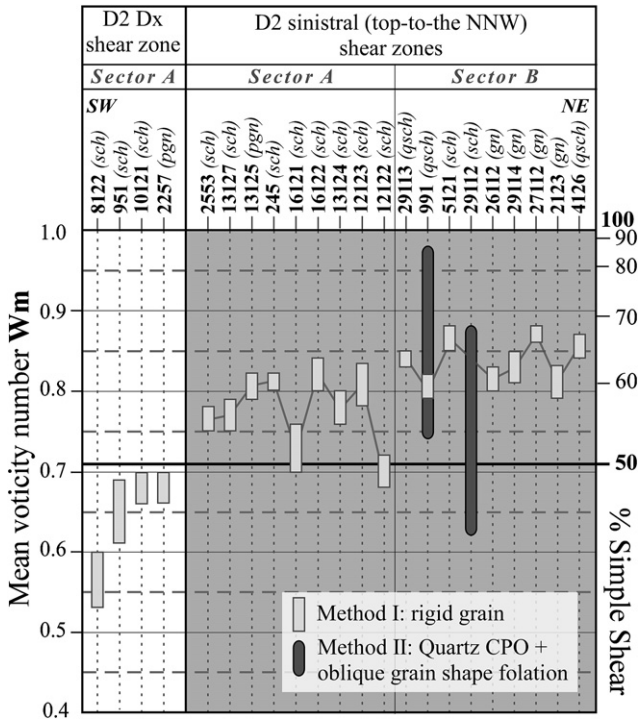

Fig. 10. Bar chart showing kinematic vorticity values estimated by rigid object (Method I: grey bars) and oblique grain shape – quartz c-axis fabrics (Method II: black bars) for samples from D2 dextral and sinistral shear belts. The samples were collected along a SW–NE traverse line approximately orthogonal to the shear belt margins within each sector. Relationship between vorticity number and contribution of simple shear component is indicated. Sch: schist; qsch: quartz-schist; pgn: paragneiss, gn: fine-grained gneiss.

yield lower W_m values than in Sector B, indicating a simple shear component of *c.* 49–62% ($W_m = 0.68$–0.84) with an average simple shear contribution of 55% (Fig. 10). We suggest that the lower R_c value (and therefore lower W_m estimates) recorded in Sector A may be related to later development of the phyllonites. As recently suggested by Johnson et al. (2009), the presence of abundant phyllosilicate could localized strain on the clast/matrix boundary, leading a reduction in the R_c value.

In the dextral shear belt estimated Method I W_m values range from 0.53 to 0.70 with an average W_m value of 0.63 indicating a simple shear component of less than 50% of the total deformation (Fig. 10). Because of the diffuse presence of S/C–S/C′ fabrics, most of the samples collected in the dextral shear belt, even if C′ planes are in agreement with a component of coaxial deformation, do not strictly satisfy the assumptions of the vorticity measurement techniques, particularly with respect to homogeneity of deformation/flow.

7. Discussion

Microstructural analyses, quartz petrofabric measurements and estimated flow vorticities indicate a significant change in the kinematics and deformation conditions in the central sector of the Variscan axial belt in Sardinia, during the D2 post-collisional stage.

A Barrovian metamorphic mineral assemblage (kyanite, staurolite, garnet and plagioclase) was deformed both in the dextral and sinistral shear belts. This implies that motion on these shear belts commenced after peak metamorphism (Fig. 11). In addition, the P–T–t path, as well as the growth of sillimanite, parallel and oblique to the S2 mylonitic foliation within the sinistral shear zones, suggest that the high-grade metamorphic rocks were affected by nearly isothermal exhumation during or after sinistral shearing. Estimated

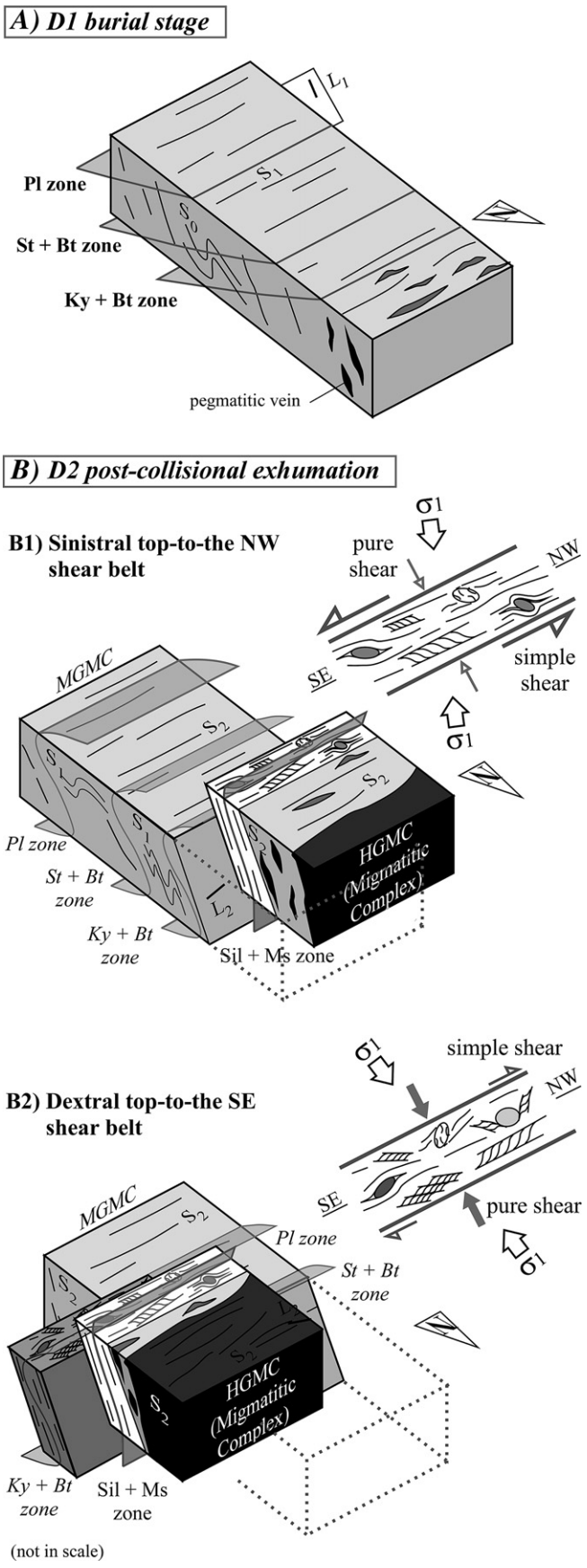

Fig. 11. Schematic block diagrams illustrating geometry and kinematics of the study area. (a) D1 burial stage produced S1 foliation, SW verging folds and down-dip stretching lineation (L1) which is compatible with tectonic model involving frontal collision sub-orthogonal to trend of the belt (i.e. NE–SW). During the burial stage pegmatitic veins and local partial melt events became more intense traced toward the deepest sectors of nappe (the future HGMC) and the main Barrovian isograds developed. (b) D2 post-collisional stage produced folding and shearing domains oriented parallel to the trend of belt. The shearing domains developed initially with a sinistral sense of motion close to a simple shear regime producing early stages of exhumation of the deeper metamorphic rocks. The HGMC underwent nearly isothermal exhumation along a path that intersects the sillimanite stability field (b1). During later stages of exhumation at higher crustal levels (i.e. in the MGMC) the location and sense of shearing changed producing the dextral shear belt dominated by pure shearing, always parallel to the trend of the belt (b2). A change of the regional stress field, of *c.* 30° counter-clockwise from SW–NE to S–N, which may be due to: (1) rotation of the convergence direction during continental collision and/or, (2) irregularities in the continental margins and/or, (3) the progressive bending of the Ibero-Armorican Arc, could be responsible for changes in both kinematics and vorticity of flow in this sector of the Variscan belt.

deformation temperatures from quartz and feldspar deformation microstructures and from quartz c-axis fabrics corroborate the high deformation temperatures indicated by the preserved mineral assemblage. The widespread presence of myrmekites, often with asymmetric microstructures oriented perpendicularly to the shortening direction, in the sinistral mylonites, suggests that sinistral shearing may have occurred during retrograde metamorphism associated with the initial stages of exhumation.

Estimated flow vorticities along the sinistral mylonites indicate the significant role played by simple shear during initial exhumation of the HGMC (Fig. 10). This interpretation is supported by quartz petrofabric analyses that indicate dominant non-coaxial deformation under plane strain conditions. Quantitative vorticity analyses carried out on the D2 dextral shear belt indicate a major component of pure shear component that reaches about 60% of total deformation. However, although based on a relative small number of samples, our W_m estimates are in good agreement with those calculated in the western and eastern sections of the PAL that are only affected by dextral shearing. According to Carosi and Palmeri (2002) and Iacopini et al. (2008), the dominant pure shear in these two sections reaches 50–77% of the total deformation with W_m estimates ranging from $0.55/0.65 \pm 0.25$ in Nurra and southern Asinara Island, to 0.35 ± 0.25 in northern Asinara Island and to 0.5–0.7 in the Baronie region. In addition, Type-II cross-girdle quartz c-axis fabrics from the dextral mylonites indicate a dominant coaxial (pure shear) deformation that developed under plane strain to slightly constrictional strain conditions. The presence of conjugate shear bands with opposite shear senses is compatible with flow within a dominant coaxial regime (Fueten et al., 1991; Kurz and Northrup, 2008).

Based on the collected data, we divide the D2 post-collisional phase into two main stages.

(1) the presence of mylonitic pegmatite veins and migmatites in the HGMC indicates the presence of local partial melt during the early stages of D2 deformation. At this stage, strain softening processes led to localize shear deformation in the HGMC (Fig. 11b) producing sinistral kinematic framework active under a simple shear-dominate regime. The lack in Sector B both of long-lived dextral shearing and well-developed F3 folds, led us to assume the plunge toward S–SE of L2 mineral lineation (documented in that sector) as representative for the sinistral shear belt system. As consequence the strike-slip component of transpression produced a top-to-the NNW movement, whereas the dip-slip component produced the early extrusion of the HGMC onto the MGMC;
(2) During the second stage of D2 deformation, shear deformation moved to a new location (i.e. in the MGMC), changing kinematics and flow type (Fig. 11c). Dextral shear deformation

occurred under a pure-shear-dominated regime that enhanced extrusion of the HGMC and produced a telescoping of the Barrovian isograds that in map view is marked by a condensed transition within 2 km from biotite to biotite + kyanite zones. Our data indicate the presence during the D2 deformation phase, of a general non-coaxial flow with an initially significant component of simple shear that switched to a dominant coaxial component during dextral shearing.

Although the presence of sinistral shear zones wrapped by dextral mylonites reveals that sinistral shearing began before the dextral shearing, this does not preclude the possibility that both domains were simultaneously active during at least part of the deformation history, possibly at slightly different structural levels. This may be supported by similar P–T conditions (Carosi et al., 2009) and by the presence of similar ductile–brittle structures in the sinistral mylonites and in the easternmost samples of dextral mylonites. As a consequence, the contemporaneous movement of the two systems of shear belts would have enhanced oblique motion of material that can be factorized into two main components: a) a component of strike-slip shearing, indicated by shallowly plunging stretching lineation in the mylonites, that produced the horizontal and orogen-parallel displacement; b) a dip-slip component of deformation with vertical exhumation and shortening perpendicular to the shear zones boundaries, as indicated by F2 upright folds with fold hinges parallel to the mineral lineation and by an S2 foliation oriented sub-vertical and parallel to the shear zone boundaries.

In this view, the material extruded toward the SE between the dextral and sinistral shear belts could act as a weakness or "channel" at upper crustal levels that, enhancing fluid circulation and strain softening mechanisms, localized strain along a narrow band (i.e. the high-strain phyllonites) developed between the shear zones.

Considering the km-scale length of the shear zones, the dip-slip component potentially provides an important contribution to exhumation of the metamorphic complexes. A minimum value for the vertical component of displacement associated can be calculated using the plunge of the L2 lineation and the known minimum length of the shear zones (shown on the geological maps in Fig. 1b) under both the post-Variscan cover and the Variscan batholith.

As a consequence, considering an average plunge of 20–25° toward SE and a minimum length of 9 km for the sinistral shear belt (Fig. 1b) we estimated a minimum vertical exhumation of *c.* 3.4–4.2 km. This assumes that: a) lineation developed parallel to tectonic transport within the shear zone and, b) the combined strain and motion on the bounding faults was of sufficient magnitude for translation to be at least equal to line length measured parallel to lineation along the exposed length of the shear zone. In the same way we estimated a vertical exhumation of *c.* 1 km for the dextral shear zone. Nevertheless, P–T trajectories suggested by Carosi et al. (2009) for the study area revealed that the D2 exhumation is even greater. Coupling microstructural observation and P–T trajectories we can predict a minimum exhumation of *c.* 10 km and *c.* 10–15 km respectively for the MGMC and HGMC.

Even if the dextral shear belt crops out for only 2 km in the study area, it is worth mentioning that it has also been documented for several tens of kms across northern Sardinia from the Baronie region, in the east, to the Nurra–Asinara region in the west (Fig. 1). Petrological and geochronological data collected in these areas (Carosi and Palmeri, 2002; Di Vincenzo et al., 2004; Carosi et al., 2004) indicate for the prograde stage of D2 deformation phase, a minimum decompression of 12–15 km (*c.* 0.4–0.5 GPa) within a 15 million year time interval. Numerical simulation carried out by Iacopini et al. (2008), corroborates these values, estimating *c.* 20 km of exhumation in about 10 million years.

8. Conclusion

1) New structural, textural and quartz petrofabrics analyses within the two crustal-scale shear belts from SW Gallura region reveal that they became active at different times and at different structural levels during the D2 post-collisional deformation phase.
2) Quantitative vorticity analyses, in conjunction with quartz-fabric data and microstructural analyses, indicate that deformation within both the sinistral and dextral shear belts involved general non-coaxial flow with contemporaneous contributions of pure and simple shear. Our data suggest that the contribution of simple shear changed with time: the sinistral mylonites developed during a simple-shear-dominated regime whereas the later dextral mylonites developed under pure-shear-dominated regime.
3) The parallelism between L2 mineral lineations, F2 fold axes, the margins of D2 shear belts and steeply dipping F2 fold axial planes indicate that the coaxial component of shortening acted sub-horizontal and orthogonal to the strike of the shear belts. This caused oblique extrusion and exhumation of material during a deformation phase dominated by transpression.
4) The temporal variations in kinematics, flow type and finite strain indicate a regional change in the stress field during post-collisional orogen-parallel displacement of the continental margins caught up in the Variscan orogeny. The change from sinistral to dextral kinematics (coupled with a change in flow type and strain geometry) implies that the regional stress field may have been changed during the post-collisional exhumation stage. This may be related to: (a) rotation of the convergence direction during continental collision and/or (b) irregularities in the original continental margin and/or (c) progressive bending of the Ibero-Armorican Arc (Dias and Ribeiro, 1995; Carosi and Palmeri, 2002).

Acknowledgment

We thank an anonymous reviewer and J. Carreras for their helpful comments and criticism.

Appendix. Supplementary material

Supplementary data associated with this article can be found, in the online version, at doi:10.1016/j.jsg.2009.10.001.

References

Bailey, C.M., Polvi, L.E., Forte, A.M., 2007. Pure shear dominated high-strain zones in basement terranes. In: Hatcher, R.D., Carlson, M.P., McBride, J.H., Martinez Catalan, J.R. (Eds.), 4-D Framework of Continental Crust. Geological Society of America Memoir, vol. 200, pp. 93–108.

Bouchez, J.L., 1977. Plastic deformation of quartzite at low temperature in an area of natural strain gradient. Tectonophysics 39, 25–50.

Cappelli, B., Carmignani, L., Castorina, F., Di Pisa, A., Oggiano, G., Petrini, R., 1992. A Hercynian suture zone in Sardinia: geological and geochemical evidences. Geodinamica Acta 5, 101–118.

Carmignani, L., Carosi, R., Di Pisa, A., Gattiglio, M., Musumeci, G., Oggiano, G., Pertusati, P.C., 1994. The Hercynian chain in Sardinia (Italy). Geodinamica Acta 7, 31–47.

Carosi, R., Di Pisa, A., Iacopini, D., Montomoli, C., Oggiano, G., 2004. The structural evolution of the Asinara Island (NW Sardinia, Italy). Geodinamica Acta 17 (5), 309–329.

Carosi, R., Frassi, C., Iacopini, D., Montomoli, C., 2005. Post-collisional transpressive tectonic in northern Sardinia. In: Carosi, R., Dias, R., Iacopini, D., Rosenbaum, G. (Eds.), The Southern Variscan Belt. Journal of Virtual Explorer. ISSN: 1441-8142 ISSN: 1441-8142, 1–18. 19, Paper 4.

Carosi, R., Frassi, C., Montomoli, C., 2009. Deformation during exhumation of medium- and high-grade metamorphic rocks in the Variscan chain in northern Sardinia (Italy). Geological Journal 44, 280–305.

Carosi, R., Montomoli, C., Visonà, D., 2007. A structural transect in the Lower Dolpo: insights on the tectonic evolution of Western Nepal. Journal of Asian Earth Sciences 29, 407–423.
Carosi, R., Oggiano, G., 2002. Structural evolution of North eastern Sardinia: insight on the tectonic evolution of the Variscan belt. Comptes Rendus Geoscience 334, 287–294.
Carosi, R., Palmeri, R., 2002. Orogen parallel tectonic transport in the Variscan belt of northeastern Sardinia (Italy): implications for exhumation of medium pressure metamorphic rocks. Geological Magazine 139, 497–511.
Carreras, J., Druguet, E., 1994. Structural zonation as a result of inhomogeneous non-coaxial deformation and its control on syntectonic intrusions: an example from the Cap de Creus area, eastern-Pyrenees. Journal of Structural Geology 16, 1525–1534.
Del Moro, A., Di Simplicio, P., Ghezzo, C., Guasparri, G., Rita, F., Sabatini, G., 1975. Radiometric data and intrusive sequence in the sardinian batholith. Neues Jahrbuch fur Mineralogie Monatshefte 126, 28–44.
Di Pisa, A., Oggiano, A., Talarico, F., 1993. Post-collisional tectono-metamorphic evolution in the axial zone of the hercynian belt in Sardinia: the example from Asinara Island. Bulletin BRGM 219, 216–217.
Di Vincenzo, G., Carosi, R., Palmeri, R., 2004. The relationship between tectono-metamorphic evolution and argon isotope records in white mica: constraints from in situ 40Ar–39Ar laser analysis of the Variscan basement of Sardinia. Journal of Petrology 45, 1013–1043.
Dias, R., Ribeiro, A., 1995. The Ibero-Armorican arc. A collision effect against an irregular continent? Tectonophysics 246, 113–128.
Druguet, E., Passchier, C.W., Carreras, J., Victor, P., den Brok, B., 1997. Analysis of a complex high strain zone at Cap de Creus, Spain. Tectonophysics 280, 31–45.
Elter, F.M., Musumeci, G., Pertusati, P.C., 1990. Late Hercynian shear zones in Sardinia. Tectonophysics 176, 387–404.
Etchecopar, A., 1977. A plane kinematic model of progressive deformation in a polycrystalline aggregate. Tectonophysics 39, 121–139.
Ferrara, G., Ricci, C.A., Rita, F., 1978. Isotopic ages and tectono-metamorphic history of the metamorphic basement of north-eastern Sardinia. Contribution to Mineralogy and Petrology 68, 99–106.
Fossen, H., Tikoff, B., 1993. The deformation matrix for simultaneous pure shear, simple shear and volume change and its application to transtension and transpression tectonics. Journal of Structural Geology 15, 413–425.
Fossen, H., Tikoff, B., 1998. Forward modelling of non-steady-state deformations and the 'minimum strain path': reply. Journal of Structural Geology 20, 979–981.
Franceschelli, M., Memmi, I., Ricci, C.A., 1982. Zoneografia metamorfica della Sardegna settentrionale. In: Carmignani, L., Cocuzza, T., Grezzo, C., Pertusati, P.C., Ricci, C.A. (Eds.), Guida alla Geologia del Paleozoico Sardo. Guide geologiche regionali. Societá Geologica Italiana, pp. 137–149.
Franceschelli, M., Puxeddu, M., Cruciani, G., Utzeri, D., 2007. Metabasites with eclogite facies relics from Variscides in Sardinia, Italy: a review. International Journal of Earth Sciences 96, 795–815.
Frassi, C., 2006. The Badesi-Li Paùlis shear zones in the inner zone of the Variscan belt in Sardinia (Italy): structural analysis and regional implications. Ph.D thesis, University of Pisa.
Fueten, F., Robin, P.Y.F., Stephens, R., 1991. A model for the development of a domainal quartz c-axis fabric in a coarse-grained gneiss. Journal of Structural Geology 13, 1111–1124.
Ghezzo, C., Memmi, I., Ricci, C.A., 1979. Un evento granulitico nel basamento metamorfico della Sardegna nord-orientale. Memoria della Società Geologica Italiana 20, 23–38.
Gomez-Rivas, E., Bons, P.D., Griera, A., Carreras, J., Druguet, E., Evans, L., 2007. Journal of Structural Geology 29, 1882–1899.
Grasemann, B., Fritz, H., Vannay, J.C., 1999. Quantitative kinematic flow analysis from the Main Central Thrust Zone (NW-Himalaya, India); implications for a decelerating strain path and the extrusion of orogenic wedges. Journal of Structural Geology 21, 837–853.
Green, H.W., Griggs, D.T., Christie, J.M., 1970. Syntectonic and annealing recrystallization of fine-grained quartz aggregates. In: Paulitsch, P. (Ed.), Experimental and Natural Rock Deformation. Springer, Berlin, Heidelberg, New York, pp. 272–335.
Grujic, D., 2006. Channel flow and continental collision tectonics: an overview. In: Law, R.D., Searle, M.P., Godin, L. (Eds.), Channel Flow, Ductile Extrusion and Exhumation in Continental Collision Zones. Geological Society, London, Special Publications, vol. 268, pp. 25–37.
Grujic, D., Casey, M., Davidson, C., Hollister, L.S., Kundig, R., Pavlis, T., Schmid, S., 1996. Ductile extrusion of the Higher Himalayan Crystalline in Bhutan: evidence from quartz microfabrics. Tectonophysics 260, 21–43.
Heilbronner, R., Tullis, J., 2002. The effect of static annealing on microstructures and CPOs of quartzites experimentally deformed in axial compression and shear. In: Geological Society, London, Special Publications, vol. 200, pp. 191–218.
Heilbronner, R., Tullis, J., 2006. Evolution of c-axis pole figures and grain size during dynamic recrystallization: results from experimentally sheared quartzites. Journal of Geophysical Research 111, B10202. doi:10.1029/2005JB004194.
Herwegh, M., Handy, M.R., 1996. The evolution of high temperature mylonitic microfabrics: evidences for simple shearing of a quartz analogue (norcamphor). Journal of Structural Geology 18, 689–710.
Hippertt, J.F., 1994. Microstructures and c-axis fabrics indicative of quartz dissolution in sheared quartzites and phyllonites. Tectonophysics 229, 141–163.
Hirth, G., Teyssier, C., Dunlap, J., 2001. An evaluation of quartzite flow laws based on comparisons between experimentally and naturally deformed rocks. International Journal of Earth Sciences 90, 77–87.
Hirth, G., Tullis, J., 1992. Dislocation creep regimes in quartz aggregates. Journal of Structural Geology 14, 145–159.
Holcombe, R., Little, T., 2001. A sensitive vorticity gauge using rotated porphyroblasts and its application to rocks adjacent to Alpine fault, New Zealand. Journal of Structural Geology 23, 979–989.
Iacopini, D., Carosi, R., Montomoli, C., Passchier, C.W., 2008. Strain analysis and vorticity of flow in the northern Sardinian Variscan belt: recognition of a partitioned oblique deformation event. Tectonophysics 446, 77–96.
Iacopini, D., Passchier, C.W., Koehn, D., Carosi, R., 2007. Fabric attractors in general triclinic flow systems and their application to high strain shear zones: a dynamical system approach. Journal of Structural Geology 29, 298–317.
Jessell, M.W., Lister, G., 1990. A simulation of the temperature dependence of quartz fabric. In: Geological Society, London, Special Publication, vol. 54 pp. 353–362.
Jessup, M.J., Law, R.D., Frassi, C., 2007. The rigid grain net (RGN): an alternative method for estimating mean vorticity number (Wm). Journal of Structural Geology 29, 411–421.
Johnson, S.E., Lenferink, H.J., Price, N.A., Marsh, J.H., Koons, P.O., West, D.P., Beane, R., 2009. Clast-based kinematic vorticity gauges: the effects of slip at matrix/clast interfaces. Journal of Structural Geology 31 (12), 1472–1489.
Jones, R.R., Holdsworth, R.E., Bailey, W., 1997. Lateral extrusion in transpression zones; the importance of boundary conditions. Journal of Structural Geology 19, 1201–1217.
Jones, R.R., Holdsworth, R.E., Clegg, P., McCaffrey, K., Tavarnelli, E., 2004. Inclined transpression: the importance of boundary conditions. Journal of Structural Geology 26, 1531–1548.
Kruhl, J.H., 1998. Reply: prism- and basal-plane parallel subgrain boundaries in quartz: a microstructural geothermobarometer. Journal of Metamorphic Petrology 16, 142–146.
Kurz, G.A., Northrup, C.J., 2008. Structural analysis of mylonitic rocks in the Cougar Creek Complex, Oregon-Idaho using the porphyroblast hyperbolic distribution method, and potential use of SC′-type extensional shear bands as quantitative vorticity indicators. Journal of Structural Geology 30, 1005–1012.
Lana-Fùnez, S., 2002. Quartz c-axis texture mapping of a Variscan regional foliation (Malpica-Tui Unit, NW Spain). Journal of Structural Geology 24, 1299–1312.
Larson, K.P., Godin, L., 2009. Kinematics of the Greater Himalayan sequence, Dhaulagiri Himal: implications for the structural framework of central Nepal. Journal of the Geological Society, London 166, 25–43.
Law, R.D., 1990. Crystallographic fabrics: a selective review of their applications to research in structural geology. In: Knipe, R.J., Rutter, E.H. (Eds.), Deformation Mechanisms, Rheology and Tectonics. Geological Society, London, Special Publication, vol. 54, pp. 335–352.
Law, R.D., 1986. Relationships between strain and quartz crystallographic fabrics in the Roche Maurice Quartzites of Plougastel, western Brittany. Journal of Structural Geology 8, 493–516.
Law, R.D. Moine thrust zone mylonites at the Stack of Glencoul: II – results of vorticity analyses and their tectonic significance. In: Law, R.D., Butler, R.W.H., Holdsworth, R., Krabendam, M., Strachan R. (Eds.), Continental Tectonics and Mountain Building: The Legacy of Peach and Horne. Geological Society of London Special Publications, in press.
Law, R.D., Jessup, M.J., Searle, M.P., Cottle, J.M., Waters, D., 2008. Telescoping of isotherms beneath the South Tibetan Detachment, Mount Everest Massif: implications for magnitude of internal flow during extrusion of the Greater Himalayan Slab [extended abstract]. Himalayan Journal of Science 5, 86–87.
Law, R.D., Knipe, R.J., Dayan, H., 1984. Strain path partitioning within thrust sheets: microstructural and petrofabric evidence from the Moine thrust zone at Loch Eriboll, NW Scotland. Journal of Structural Geology 6, 477–497.
Law, R.D., Morgan, S.S., Casey, M., Sylvester, A.G., Nyman, M., 1992. The Papoose Flat pluton of eastern California: a re-assessment of its emplacement history in the light of new microstructural and crystallographic fabric observations. Transactions of the Royal Society of Edinburgh: Earth Sciences 83, 361–375.
Law, R.D., Searle, M.P., Simpson, R.L., 2004. Strain, deformational temperatures and vorticity of flow at the top of the Greater Himalayan Slab, Everest Massif, Tibet. Journal of the Geological Society, London 161, 305–320.
Law, R.D., Thigpen, J.R., Cook, B., 2007. Field excursion C – mylonites associated with the Stack of Glencoul: May 15th and 17th 2007. In: Strachan, R., Thigpen, J.R. (Eds.), Continental Tectonics and Mountain Building – the Peach and Horne Meeting. A Guide to Field Excursions, Joint meeting of the Geological Society of London and Geological Society of America, pp. 66–103.
Lin, S., Jiang, D., Williams, P.F., 1998. Transpression (or transtension) zones of triclinic symmetry: natural example and theoretical modelling. In: Holdsworth, R.E., Strachan, R.A., Dewey, J.F. (Eds.), Continental Transpressional and Transtensional Tectonics. Geological Society, London, Special Publication, vol. 135, pp. 41–57.
Lister, G.S., 1977. Crossed-girdle c-axis fabrics in quartzites plastically deformed by plane strain and progressive simple shear. Tectonophysics 39, 51–54.
Lister, G.S., Hobbs, B.E., 1980. The simulation of fabric development during plastic deformation of quartzite and its application to quartzite: the effect of deformation history. Journal of Structural Geology 2, 355–370.
Marjoribanks, R.W., 1976. The relation between microfabric and strain in a progressively deformed quartzite sequence from central Australia. Tectonophysics 32, 269–293.

Means, W.D., 1994. Rotational quantities in homogeneous flow. Journal of Structural Geology 16, 437–445.
Montomoli, C., 2003. Zone di taglio fragili-duttili nel basamento varisico metamorfico di basso grado della Nurra meridionale (Sardegna nord-occidentale). Atti Società Toscana Scienze Naturali, memorie serie A 108, 23–29.
Morgan, S.S., Law, R.D., 2004. Unusual transition in quartzite dislocation creep regimes and crystal slip systems in the aureole of the Eureka Valley-Gioshua Flat-Beer Creek pluton, California: a case for anhydrous conditions created by decarbonation reactions. Tectonophysics 384, 209–231.
Nyman, M., Law, R.D., Morgan, S.S., 1995. Conditions of contact metamorphism, Papoose Flat pluton, eastern California, USA: implications for cooling and strain histories. Journal of Metamorphic Geology 13, 627–643.
Oggiano, G., Di Pisa, A., 1992. Geologia della catena Ercinica in Sardegna – Zona Assiale. In: Carmignani, L., Pertusati, P.C., Barca, S., Carosi, R., Di Pisa, A., Gattiglio, M., Musumeci, G., Oggiano, G. (Eds.), Struttura della catena ercinica in Sardegna. Guida all'escursione. Gruppo Informale di Geologia Strutturale, Siena, pp. 147–177.
Okudaira, T., Takeshita, T., Hara, I., Ando, J., 1995. A new estimate of the conditions for transitional from basal <a> to prism <c> slip in naturally deformed quartz. Tectonophysics 250, 31–46.
Passchier, C.W., 1987. Stable positions of rigid objects in non coaxial flow – a study in vorticity analysis. Journal of Structural Geology 9, 679–690.
Passchier, C.W., 1988. Analysis of deformation path in shear zones. Geologisches Rundschau 77, 309–318.
Passchier, C.W., 1998. The monoclinic flow. Journal of Structural Geology 20, 1121–1137.
Passchier, C.W., Trouw, R.A.J., 2006. Microtectonics. Springer Verlag, Berlin-Heidelberg–New York.
Pryer, L.L., 1993. Microstructures in feldspars from a major crustal thrust zone: the Grenville Front, Ontario, Canada. Journal of Structural Geology 15, 21–36.
Ricci, C.A., Carosi, R., Di Vincenzo, G., Franceschelli, M., Palmeri, R., 2004. Unravelling the tectono-metamorphic evolution of medium-pressure rocks from collision to exhumation of the Variscan basement of NE Sardinia: a review. Special issue 2: A showcase of the Italian research in metamorphic petrology. Periodico di Mineralogia 73, 73–83.
Robin, P.Y.F., Cruden, A.R., 1994. Strain and vorticity pattern in ideally ductile transpression zones. Journal of Structural Geology 16, 447–467.
Sanderson, D., Marchini, R.D., 1984. Transpression. Journal of Structural Geology 6, 449–458.
Sarkarinejad, K., Faghih, A., Grasemann, B., 2008. Transpressional deformations within the Sanandaj-Sirjan metamorphic belt (Zagros Mountains, Iran). Journal of Structural Geology, 1–9.
Schmid, S., Casey, M., 1986. Complete fabric analysis of some commonly observed quartz C-axis patterns. American Geophysical Union 36, 263–286.
Simpson, C., 1985. Deformation of granitic rocks across the brittle–ductile transition. Journal of Structural Geology 7, 503–511.
Simpson, C., De Paor, D.G., 1997. Practical analysis of general shear zones using porphyroclast hyperbolic distribution method: an example for the Scandinavia Caledonides. In: Sengupta, S. (Ed.), Evolution of Geological Structures in Micro- and Macro-scale. Chapman and Hall, London, pp. 169–184.
Stipp, M., Stunitz, H., Heilbronner, R., Schmid, S.M., 2002a. The eastern Tonale fault zone: a 'natural laboratory' for crystal plastic deformation of quartz over a temperature range from 250 to 700 °C. Journal of Structural Geology 24, 1861–1884.
Stipp, M., Stunitz, H., Heilbronner, R., Schmid, S.M., 2002b. Dynamic recrystallization of quartz: correlation between natural and experimental conditions. In: De Meer, S., Drury, M.R., De Bresser, J.H.P., Pennock, G.M. (Eds.), Deformation Mechanisms, Rheology and Tectonics: Current Status and Future Perspectives. Geological Society, London, Special Publications, vol. 200, pp. 171–190.
Stünitz, H., 1991. Folding and shear deformation in quartzite, inferred from crystallographic preferred orientation and shape fabrics. Journal of Structural Geology 12, 71–86.
Sullivan, W.A., 2008. Significance of transport-parallel strain variations in part of the Raft River shear zone, Raft River Mountains, Utah, USA. Journal of Structural Geology 30, 138–158.
Sullivan, W.A., Law, R.D., 2007. Deformation path partitioning within the transpressional White Mountain shear zone, California and Nevada. Journal of Structural Geology 29, 583–598.
Takeshita, T., Wenk, H.R., Lebensohn, R., 1999. Development of preferred orientation and microstructures in sheared quartzite: comparison of natural data and simulation results. Tectonophysics 312, 133–155.
Ten Grotenhuis, S.M., Trouw, R.A.J., Passchier, C.W., 2003. Evolution of mica fish in mylonitic rocks. Tectonophysics 372, 1–21.
Tikoff, B., Fossen, H., 1993. Simultaneous pure and simple shear: the unified deformation matrix. Tectonophysics 217, 267–283.
Tikoff, B., Fossen, H., 1995. The limitation of three-dimensional kinematic vorticity analysis. Journal of Structural Geology 17, 1771–1784.
Tikoff, B., Teyssier, C., 1994. Strain modelling of displacement field partitioning in transpressional orogens. Journal of Structural Geology 16, 1575–1588.
Truesdell, C., 1954. The Kinematics of Vorticity. Indiana University Press, Bloomington.
Tullis, J., 1977. Preferred orientation of quartz produced by slip during plane strain. Tectonophysics 39, 87–102.
Tullis, J., Christie, J.M., Griggs, D.T., 1973. Microstructures and preferred orientations of experimentally deformed quartzites. Geological Society of America Bulletin 84, 297–314.
Vissers, R.L.M., 1993. Quartz c-axis fabrics in deformed conglomerates: some support for a skeletal approach to fabric analyses. Journal of Structural Geology 15, 1055–1060.
Wallis, S.R., 1992. Vorticity analysis in a metachert from the Sanbagawa Belt, SW Japan. Journal of Structural Geology 14, 271–280.
Wallis, S.R., 1995. Vorticity analysis and recognition of ductile extension in the Sanbagawa Belt, SW Japan. Journal of Structural Geology 17, 1077–1093.
Wallis, S.R., Platt, J.P., Knott, S.D., 1993. Recognition of syn-convergence extension in accretionary wedges with examples from the Calabrian Arc and the Eastern Alps. American Journal of Sciences 293, 463–495.
Xypolias, P., 2009. Some new aspects of kinematic vorticity analysis in naturally deformed quartzites. Journal of Structural Geology 31 (1), 3–10.
Xypolias, P., Koukouvelas, I.K., 2001. Kinematic vorticity and stain patterns associated with ductile extrusion in the Chermes shear zones (External Hellnides, Greece). Tectonophysics 338, 59–77.